Subthreshold Quantum Ballistic Current and QuantumThreshold Voltage Modeling for Nanoscale FinFET

Udit Monga and Tor A. Fjeldly

Department of Electronics and Telecommunications, Norwegian University of Science and technology,
UNIK - University Graduate Center, NO-2007, Kjeller, Norway.
Fax: +47 63818146, Phone +47 64844700, { udit, torfj}@unik.no

ABSTRACT

An analytical modeling framework for quantum ballistic charge transport in the subthreshold regime, and a quantum threshold voltage model for nanoscale double-gate (DG) FinFET are presented. For subthreshold conditions, we assume that the electrostatics of the lightly doped silicon body is dominated by the inter-electrode capacitive coupling between the body electrodes. Hence, the charge is neglected in Poisson's equation. This decouples the self-consistency between the charge transport, the quantum effects and the body electrostatics. The threshold condition is obtained by self-consistently adjusting the quantum charge potential.

Keywords: double gate FinFET, quantum effects, ballistic transport, threshold voltage, conformal mapping.

1 INTRODUCTION

As MOSFET channel dimensions shrink, effects such as the ballistic component in the drain current and quantum-mechanical confinement increases. A modeling framework capturing these effects is important because: 1) It sets out a framework for modeling of the ultimate MOSFETs. 2) It gives an insight about the ultimate performance limits.

DG structures are among the most promising MOSFET devices in future. A drift-diffusion based quantum mechanical modeling framework for UTB devices operating in the subthreshold and near-threshold regimes has already presented [1]. Here we focus on modeling the quantum ballistic current and the quantum threshold voltage in DG FinFETs. Some of the previous papers have either focused on simulation studies [2,3] or classical thermionic emission currents [4] to model such devices in the ballistic regime. In the present case, we consider ultra-thin devices (UTDs) in the subthreshold regime, where the potential distribution is modeled by solving the 2D Laplace equation using conformal mapping techniques [5,6]. To model quantum effects, we solve the 1D Schrödinger equation in the gate-to-gate (G-G) direction to obtain the eigen-functions in terms of the parabolic cylindrical functions [7].

The DG device considered here (see Fig. 1) has an insulator thickness t_{ox} = 1.6 nm, and an insulator relative dielectric permittivity ε_{ox} = 7. The doping density of the *p*-type silicon body is 10^{15}cm^{-3}. As gate material, we select a near-midgap metal with work function 4.53 eV. Idealized metal contacts with a work function of 4.17 eV (corresponding to that of *n*+ silicon) are assumed for the source and drain. This ensures equipotential surfaces on all the device contacts. To simplify the modeling, we replace the insulator by an electrostatically equivalent silicon layer of thickness $t'_{ox} = t_{ox}\varepsilon_{si}/\varepsilon_{ox}$, where ε_{si} is the relative permittivity of silicon. Hence, we define the extended body thickness as $H = W_{fin} + 2t'_{ox}$, where W_{fin} is the fin-width (silicon thickness).

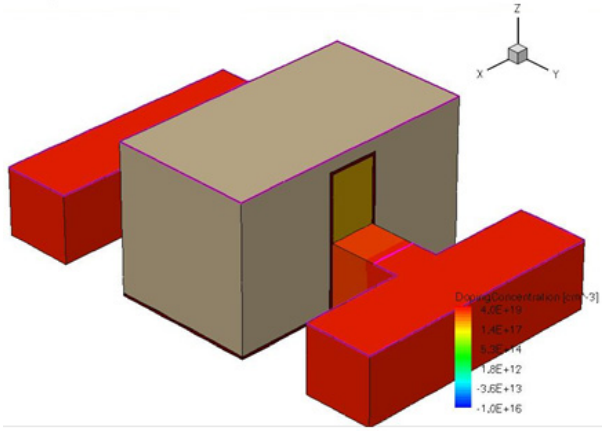

Figure 1: Schematic representation of DG FinFET

2 QUANTUM MODELING

Due to separation of the top electrode by a hard mask, the potential variation along the fin height in DG FinFETs is negligible and thus 2D DG solutions can be directly applied to this 3D structure. The effect of height on quantum confinement does become important for relatively short fin heights (H_{fin} < 20nm) [8], but here we consider higher, more practical devices, with sufficient current drivability.

To model the potential in the subthreshold regime, we use conformal mapping techniques to solve the Laplace equation [5]. To obtain a simplified distribution, we assume parabolic potential distribution in the gate-to-gate (G-G) (x) direction. This has been shown to be a good approximation in the subthreshold regime [6] and the Laplace potential can be represented as:

$$\varphi_L(x,y) \approx \varphi_c(y)\left(1-\frac{4x^2}{H^2}\right)+V_{gs}-V_{FB} \quad (1)$$

where $\varphi_c(y)$ is the difference between the Laplace potential at position y on the source-drain (S-D) symmetry line and that of the gate-silicon interface of the extended body. V_{gs} is the gate-source potential, and V_{FB} is the flat-band voltage of the gate.

Using the above expression for the potential in the Schrödinger equation, we have [1]:

$$-\frac{\hbar^2}{2m_x^*}\frac{d^2\psi(x)}{dx^2}+\left[q\varphi_c(y)\left(\frac{2x}{H}\right)^2\right]\psi(x)=E\psi(x) \quad (2)$$

This can be expressed in terms of the standard equation of parabolic cylinder functions [8] given as:

$$\frac{d^2\psi(t)}{dx^2}-(\frac{1}{4}t^2+v)\psi(t)=0 \quad (3)$$

where $t=\alpha x$, $\alpha=\left[32m_x^*q\varphi_c(y)/(H\hbar)^2\right]^{1/4}$, v = E/$\beta$, and $\beta=\hbar\sqrt{8q\varphi_c(y)/H^2m_x^*}$

This equation has both even and odd solutions. As the potential is symmetric about $x = 0$, the wave function must have a definite parity and thus $\psi(t)$ is given by two different polynomials with even and odd terms:

$$\psi_{e,o}(t)=A_e(1+\sum_{n(even)=2}^{\infty}c_nt^n/n!),A_o(t+\sum_{n(odd)=3}^{\infty}c_nt^n/n!) \quad (4)$$

where A_e and A_o are normalization constants and the coefficients c_n are determined from the recursive relation given in [8]. Depending upon the value of t, these eigenvalues can be determined by truncating the above polynomials to some higher term and then finding the numerical solution. For ultra-thin devices operating in subthreshold and near-threshold regimes, the first four terms of the polynomials give sufficient accuracy in the calculation of the lowest subbands. Since higher subbands are not affected by the potential perturbation, they can be better approximated by the eigenvalues of a particle in a box.

For devices operating in the near-threshold regime, the eigenvalues and eigenfunctions approach structure dependent values. In this case, the eigenfunction and eigenvalue corresponding to the first unprimed subband are given as:

$$\psi_1(x)=\sqrt{\frac{15}{8t_{si}}}\left(1-\frac{4x^2}{W_{fin}^2}\right) \quad (5)$$

$$E_1=\frac{4\hbar^2}{m_l^*W_{fin}^2} \quad (6)$$

3 BALLISTIC CURRENT MODELING

The charge transport is in the y-direction, and thus the net current, is the difference between the positive flux (filling positive k_y states) emitted by the source at the top of the barrier and the negative flux (filling negative k_y states) emitted by the drain at the top of the barrier. The net current can thus be evaluated by using Natori's formalism given as [9]:

$$I_d=\frac{H_{fin}q}{\hbar^2}\left(\frac{kT}{\pi}\right)^{3/2}\sum_v\sum_j\sqrt{m_z}g_v\ln\left[\frac{1+e^{-\frac{E_j(y_m)-E_{FS}}{kT}}}{1+e^{-\frac{E_j(y_m)-E_{FS}+qV_{DS}}{kT}}}\right], \quad (7)$$

where E_{FS} is the Fermi level at the source and V_{DS} is the applied drain-source voltage. It is assumed that any electron with energy higher than that of the top of the barrier has a transmission probability of 1, and any electron with lesser energy has a transmission probability of 0 (i.e. no tunnelling). The total charge-sheet density at the top of the barrier becomes:

$$Q_m=\left(\frac{qkT}{2\pi\hbar^2}\right)\sum_{valleys}\sum_j\sqrt{m_ym_z}g_v\ln\left\{\left[1+e^{-\frac{E_j(y_m)-E_{FS}}{kT}}\right]\times\left[1+e^{-\frac{E_j(y_m)-E_{FS}+qV_{DS}}{kT}}\right]\right\} \quad (8)$$

where y_m is the position of the top of the barrier, calculated using conformal mapping techniques [6,7].

In general, the total potential inside the silicon body is given as:

$$\varphi(x,y)\approx\varphi_L(x,y)+\varphi_Q(x,y) \quad (9)$$

where φ_Q is the potential due to the charge carriers. In the above-threshold regime, the negative flux from the drain at the top of the barrier decreases when drain voltage is applied. This results in a reduction of the total charge density at this location. Due to this reduction in the charge density, the negative potential φ_Q decreases. In turn, this increases the total potential. (We note that drain induced barrier lowering (DIBL) also gives rise to a slight potential increase, but this effect vanishes in the strong-inversion regime [6]). The net effect is that the positive flux from the source side increases. In the subthreshold regime, however, the potential is fixed by the bias voltages of the contacts and thus we actually see a reduction of charge at the barrier maximum by approximately a factor of two at sufficiently high drain voltages (in reality, we always have a factor of

less than two because of the DIBL effect in the subthreshold regime).

Figure 2 shows the modeled current for a 5 nm thick device, compared with ballistic NEGF (non-equilibrium Green's function) simulations and constant-mobility DD (drift-diffusion) simulations, both performed using the ATLAS device simulator.

It is of interest to note that in subthreshold the constant-mobility DD mechanism gives rise to similar characteristics as those of the ballistic model, except for a shift in magnitude. For UTBs, the major contribution to the drain current comes from the lowest subband, and thus (7) for the non-degenerate case can be written as:

$$I_d = H_{fin} q \frac{n_m}{2} \sqrt{\frac{2kT}{\pi m_t^*}} \left\{ 1 - \exp\left(-\frac{V_{ds}}{V_{th}} \right) \right\} \tag{10}$$

where n_m is the electron density from the lowest subband at the top of the barrier and m_t^* is the transverse effective mass. The drift-diffusion current for the same case can be expressed as [10]:

$$I_d = H_{fin} n_m \frac{\mu_n kT}{L_\sigma} \left\{ 1 - \exp\left(-\frac{V_{ds}}{V_{th}} \right) \right\} \tag{11}$$

where μ_n is the electron mobility and the length L_σ is the distance from the top of the barrier to where charge-sheet density has increased by a factor of '*e*'(obtained from conformal mapping analysis). Comparing the above two equations, we observe that both equations are essentially the same, except for the effective velocity at the top of the barrier. In the case of ballistic transport, the effective velocity is the thermal velocity determined by the source and the height of the barrier, and is given as:

$$v_{th} = \frac{1}{2} \sqrt{\frac{2kT}{\pi m_t^*}} \left\{ 1 - \exp\left(-\frac{V_{ds}}{V_{th}} \right) \right\} \tag{12}$$

whereas in the case of constant mobility DD, the effective velocity at the top of the barrier is the diffusion velocity and given as:

$$v_d = \mu_n \left(\frac{V_{th}}{L_\sigma} \right) \left\{ 1 - \exp\left(-\frac{V_{ds}}{V_{th}} \right) \right\} \tag{13}$$

4 QUANTUM THRESHOLD VOLTAGE MODELING

The threshold voltage V_T is defined as the value of gate voltage (for V_{ds} = 0 V) for which the transition between volume inversion and surface inversion takes place [6].

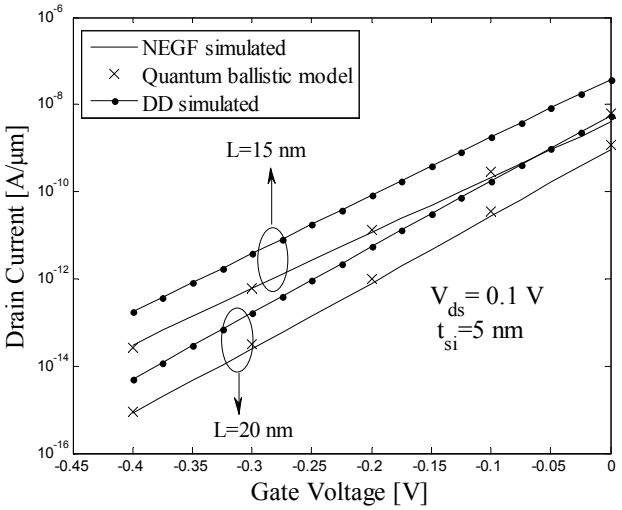

Figure 2: Comparison of modeled and numerically simulated subthreshold I_{ds}-V_{gs} characteristics for different channel lengths at V_{ds}=0.1 V

At $V_{gs} = V_T$, the electrostatic effects of capacitive coupling and free charges are nearly equal and opposite and the center potential becomes equal to V_T - V_{FB}. Thus, at threshold we have:

$$\varphi_{Qm0} + \varphi_{Lm0} \approx V_T - V_{FB} \tag{14}$$

where φ_{Qm0} and φ_{Lm0} are the values of the Laplace and charge components at the potential minimum, which will be at the device center (y = 0) for V_{ds} = 0 V. From the analytical solution for the inter-electrode body potential using the conformal mapping technique, we obtain:

$$\varphi_{Lm0} = \left[1 - \frac{4}{\pi} \tan^{-1}\left(\sqrt{k} \right) \right] \left(V_{bi} + V_{FB} - V_{gs} + \tfrac{1}{2} V_{ds} \right) \tag{15}$$

The corresponding threshold voltage based on the classical theory for DG MOSFET can be expressed in the form of a Lambert function [6].

However, for UTB devices, this solution overestimates the threshold voltage. By including the quantum effects, in combination with (14), we can get an expression for quantum threshold voltage. To include the quantum effects, we solve for the quantum charge potential φ_{Qm0} by considering the 1D Poisson's equation along the G-G axis [1]:

$$\frac{d^2 \varphi_Q(x)}{dx^2} = \frac{q}{\varepsilon_s} \sum_{valleys} \sum_j g_v N_{2D} \ln\left[1 + e^{\frac{E_F(y) - E_j(x)}{k_B T}} \right] \left| \psi_j(x) \right|^2 \tag{16}$$

Again, the threshold voltage can be expressed in form of the Lambert function as:

$$\frac{V_{bi}-V_T+V_{FB}}{k_BT/q}\exp\left(\frac{V_{bi}-V_T+V_{FB}}{k_BT/q}\right)=\lambda\exp\left(\frac{qV_{bi}}{k_BT}\right) \quad (17)$$

where λ is given as:

$$\lambda=-\frac{15\pi q}{16V_{th}\varepsilon_{si}W_{fin}}\frac{\sum_{valleys}\sum_{j}g_vN_{2D}e^{-\frac{E_j+E_g/2+q\varphi_b-q\varphi_i}{kT}}}{\pi/2-2\tan^{-1}\left(\sqrt{k}\right)}\left(\frac{11W_{fin}^{\ 2}}{120}+\frac{4W_{fin}t_{ox}^{'}}{5}\right) \quad (18)$$

Figure 3 shows the modeled threshold voltage compared with the self-consistent Poisson-Schrödinger numerical simulations done using the ATLAS device simulator. The model shows good agreement with the numerical simulations. The small deviation is due to undulations in the G-G potential present at threshold.

5 CONCLUSION

We have developed a compact quantum ballistic current model for nanoscale DG FinFET in the subthreshold regime. It is shown that constant-mobility transport model gives similar characteristics as those of the ballistic transport model. An analytical model for quantum-threshold voltage is also presented. It is shown that quantum confinement enhances the threshold voltage.

ACKNOWLEDGMENT

The work was carried out with support by the European Commission, under Grant Agreement 218255 (COMON), and the Norwegian Research Council under contracts 159559/130 (SMIDA) and 970141669 (MUSIC). The Atlas simulator was donated by Silvaco Inc.

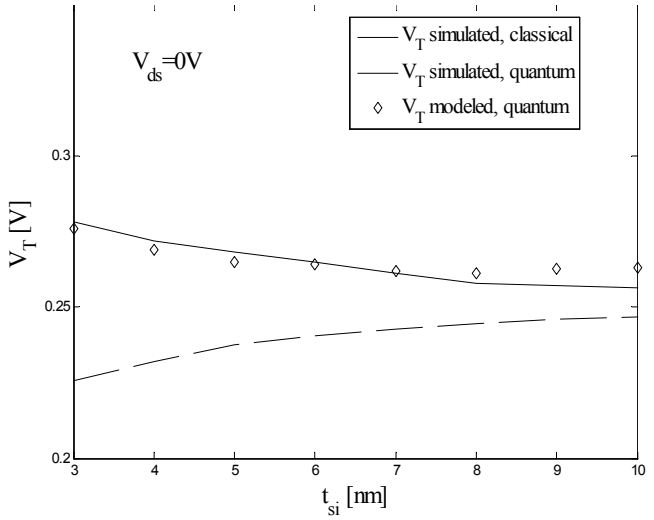

Figure 3: Comparison of modeled and numerically simulated quantum V_T variation with t_{si} for a 25 nm long device.

REFERENCES

[1] Udit Monga and Tor A. Fjeldly, "Compact Quantum Modeling Framework for Nanoscale Double-Gate MOSFET," Proc. NSTI-Nanotech 2009,Houston , Tx, May 3-7, 2009, vol. 3, pp. 580-583.

[2] R. Gusmeroli, A.S. Spinelli, "Performance Improvement of Ballistic Double-Gate Devices and Design Trade-Offs," EuroSimE 2006, pp. 1-4, April 2006.

[3] D. Munteanu and J. L. Autran, "Two-dimensional modeling of quantum ballistic transport in ultimate double-gate SOI devices," Solid-State Electronics, vol. 47, pp. 1219-1225, July 2003.

[4] Hak Kee Jung and Sima Dimitrijev, "Analysis of Subthreshold Carrier Transport for Ultimate DGMOSFET," IEEE Trans. Electron Devices, vol. 53, pp. 685-691, April 2006.

[5] T. A. Fjeldly, S. Kolberg, and B. Iniguez, "Precise 2D compact modeling of nanoscale DG MOSFETs based on conformal mapping techniques," Proc. NSTI-Nanotech 2006, Boston, MA, May 7-11, 2006, vol. 3, pp. 668-673.

[6] S. Kolberg, Modeling of electrostatics and drain current in nanoscale double-gate MOSFETs, PhD thesis, Norwegian University of Science and Technology, 2007.

[7] Milton Abramowitz and Irene A. Stegun, Handbook of Mathematical Functions with Formulas, and Mathematical tables, Dover publications, 1965.

[8] U. Monga, T.A. Fjeldly, S.K Vishvakarma, "Modeling of quantum mechanical effects in ultra-thin body nanoscale double-gate FinFET," 2nd International Workshop on Electron Devices and Semiconductor Technology, 2009. IEDST '09.

[9] K. Natori, "Ballistic MOSFET Reproduces Current–Voltage Characteristics of an Experimental device," IEEE Electron Device Letters, vol. 23, pp. 655-657, Nov. 2002.

[10] U. Monga, H. Børli, T. A. Fjeldly, "Compact subthreshold current and capacitance modeling of short-channel double-gate MOSFETs," Mathematical and Computer Modeling, vol. 51, no. 7-8, pp. 901-907, 2010.